Precracked Reinforced Concrete T-Beams Repaired in Shear with Prestressed Carbon Fiber-Reinforced Polymer Straps

Dirar, Samir; Lees, Janet M.; Morley, Chris

DOI:
10.14359/51685838

Document Version
Peer reviewed version

Citation for published version (Harvard):
Dirar, S, Lees, JM & Morley, C 2013, 'Precracked Reinforced Concrete T-Beams Repaired in Shear with Prestressed Carbon Fiber-Reinforced Polymer Straps', *ACI Structural Journal*, vol. 110, no. 5, 110-S71, pp. 855-866. https://doi.org/10.14359/51685838

PRECRACKED RC T-BEAMS REPAIRED IN SHEAR WITH PRESTRESSED CFRP STRAPS

Samir Dirar, Janet M. Lees and Chris T. Morley

Samir Dirar is a Lecturer in Structural Engineering at the University of Birmingham, United Kingdom (UK). His research interests include strengthening of existing structures with fiber reinforced polymers, finite element analysis of concrete structures and resilient structures.

Janet M. Lees is a Senior Lecturer in Structural Engineering at Cambridge University, UK. She is interested in the use of advanced durable materials as prestressing tendons for concrete elements, strengthening and repair of existing structures and advanced numerical analyses.

Chris T. Morley is a former Senior Lecturer at Cambridge University, UK. He has always been interested in plasticity theory, and especially in its application to reinforced concrete (RC) structures. His research interests extend to nonlinear finite element analysis of RC structures.

ABSTRACT

The results of an experimental and numerical investigation involving unstrengthened reinforced concrete (RC) T-beams as well as precracked RC T-beams strengthened in shear with prestressed carbon fiber reinforced polymer (CFRP) straps are presented and discussed. The results provide insights into the influence of load history and beam depth on the structural behavior of both the unstrengthened and strengthened beams. The strengthened beams exhibited capacity enhancements of 21.6% to 46% compared to the equivalent unstrengthened beams, demonstrating the potential effectiveness of the prestressed CFRP strap system. Nonlinear finite element (FE) predictions, which incorporated the load history, reproduced the observed experimental behavior but either underestimated or overestimated the post-cracking stiffness of the beams and strap strain at higher load levels. These limitations were attributed to the concrete shear models used in the FE analyses.

Keywords: beam; concrete; finite element; FRP; precracking; shear; straps; strengthening

INTRODUCTION

The typical design life of many reinforced concrete (RC) structures is several decades. During such a long life, the shear strength of a RC structure can deteriorate due to several factors including aggressive exposure conditions, natural or man-made extreme events, steel reinforcement corrosion and poor initial design. Even if no deterioration occurs, the need to sustain heavier loads and more stringent assessment codes can cause a RC structure to be judged as having deficient shear capacity. Replacing every strength-deficient structure is not only impractical, but also has serious economic consequences. Conversely, strengthening can be a more practical solution that may be implemented, possibly while the structure is being utilized, to overcome the issue of strength deficiency. One possible strengthening technique is the adhesive bonding of external fiber reinforced polymer (FRP) plates to the surface of a RC structure. FRPs are advantageous since the combination of high-strength, high-stiffness structural fibers with low-cost, lightweight, environmentally-resistant polymers results in composite materials with excellent mechanical and durability properties.

To date, FRP shear reinforcing systems have primarily been applied as externally bonded unidirectional[1] or bi-directional FRP sheets[2], laminated FRP sections[3], or passive near-surface mounted (NSM) reinforcement[4]. In these systems, the FRP reinforcement is passive and will not influence the shear behavior until the concrete has cracked, or existing cracks widen further. Proper anchorage is also essential since the bonded FRP reinforcement debonds from the concrete at a stress level of 20% to 30% of the ultimate strength of the FRP reinforcement. A higher effectiveness can be achieved when the FRP reinforcement is prestressed[5].

The prestressed carbon FRP (CFRP) straps[6] used in this study consist of unidirectional carbon fibers embedded in a thermoplastic resin to create a 12 mm (0.47 in.) wide by 0.16 mm (0.0063 in.) thick tape. Layers of the tape are wrapped around a beam and the outermost layer of the tape is then welded to the next outermost layer by melting the thermoplastic matrices of the two layers together over a length of approximately 90 mm (3.54 in.). This weld creates a closed outer loop, against which the inner loops tighten, allowing each loop to carry an equal amount of tension when stressed.

The prestressing of the strap system not only resists crack opening but also reduces the strain in the internal shear links. Previous research work[7] on the use of the CFRP straps as external shear reinforcement provided valuable findings, particularly with regard to the effects of the strap spacing, strap stiffness and level of prestressing force in the strap on the shear strength enhancement. A strap installation technique[8] that does not require access to the top surface of the beam was also developed. The long-term behavior of the straps[9] was investigated and an analytical model for predicting the contribution of the straps to the shear force capacity[10] was proposed. However, other parameters that may also influence the strengthened behavior, such as the effect of a pre-existing crack state, have not yet been studied. In practice, structures requiring strengthening will have been subjected to a complex load history and may well be carrying significant dead loads while being strengthened. An understanding of these effects is of particular importance in FRP reinforcing systems since, unlike steel, FRPs are elastic and do not yield, eventually failing in a brittle manner with little energy absorption. The aim of this study is to investigate the effect of load history and beam depth on the behavior of precracked RC T-beams repaired in shear with prestressed CFRP straps. A companion study on bonded fabric strengthened beams has been reported elsewhere[11].

RESEARCH SIGNIFICANCE

Shear strengthening of existing RC structures with prestressed CFRP straps is an area with great potential. The unbonded straps are not susceptible to debonding and development length issues. In addition, the prestressed straps provide active confinement to the concrete, which will enhance the shear capacity of the beam. However, the effect of load history on the strengthened behavior has not been studied yet. In addition to investigating the effect of load history on the shear strength enhancement, this study simulates aspects of the in-service behavior of the CFRP strap-strengthened beams including precracking and strengthening under load.

EXPERIMENTAL INVESTIGATION

Specimens and materials

The experimental program consisted of tests on two unstrengthened and four CFRP strap-strengthened RC T-beams. The beams were referenced using the notation U (unstrengthened) or S (strengthened)/effective beam depth (mm)/loading pattern/percentage of tension steel reinforcement ($A_s/b_w d$). All beams had a shear span (a) to effective depth (d) ratio of 3.8, web width (b_w) of 105 mm (4.13 in.), flange width (b_f) of 250 mm (9.84 in.) and flange thickness (t_f) of 105 mm (4.13 in.) but two different beam depths, 350 mm (13.78 in) or 270 mm (10.63 in), were considered.

The cross-sections and the internal reinforcement details are shown in **Fig. 1**. The longitudinal compression steel, Ø8 mm (Ø0.31 in.) bars, and the internal transverse steel, Ø6 mm (Ø0.24 in.) links, were the same for all the beams. However, the longitudinal tension steel differed and consisted of two Ø25 mm (Ø0.98 in.) and two Ø16 mm (Ø0.63in.) deformed bars in the 350 mm (13.78 in.) deep beams, and two Ø20 mm (Ø0.79 in.) and two Ø16 mm (Ø0.63 in.) deformed bars in the 270 mm (10.63 in.) deep beams. This represented a longitudinal reinforcement ratio of around 4.5% for each beam depth. All tested shear spans had Ø6 mm (Ø0.24 in.) internal steel transverse reinforcement spaced at 250 mm (9.84 in.) center-to-center. For the strengthened beams, the external shear reinforcement on a tested shear span consisted of three CFRP straps spaced at 200 mm (7.87 in.) center-to-center (see **Fig. 2**). Each strap had a cross-sectional area of 57.6 mm^2 (0.0893 in^2) made up of 15 layers of CFRP tape.

Based on tensile tests, the yield strength and ultimate strength values for the Ø6 mm (Ø0.24 in.), Ø8 mm (Ø0.31 in.), Ø16 mm (Ø0.63 in.), Ø20 mm (Ø0.79 in.) and Ø25 mm (Ø0.98 in.) reinforcement bars in units of MPa (ksi) were 580 (84.12), 520 (75.42), 500 (72.52), 580 (84.12), 440 (63.82) and 586 (84.99), 594 (86.15), 593 (86.01), 680 (98.63), 540 (78.32) respectively. Since many existing structures were constructed decades previously, a relatively low 28 day cube compressive strength of 25 MPa (3.63 ksi) was targeted in order to simulate typical strengths in older structures now requiring strengthening. Tensile tests carried out in the laboratory showed that the CFRP straps had

a modulus of elasticity of 121 GPa (17550 ksi), an ultimate stress of 1544 MPa (224 ksi) and a rupture strain of 0.0127.

Hoult and Lees[8] developed a CFRP strap installation technique for existing beams where vertical as well as 30° inclined holes were drilled into the flange as shown in **Fig. 1**. A strip of polytetrafluoroethylene (PTFE) was placed in the holes to serve as a form for the groove illustrated in **Fig. 1** and the holes were grouted. Once the grout had hardened the PTFE strip was removed and the CFRP strap was installed in the formed groove. In order to simulate this strap installation technique, PTFE strips were cast into the concrete and removed three days after casting, leaving grooves cast in the concrete (i.e. cast-in-place grooves) to allow the straps to pass through. Since Hoult and Lees[8] found that there was 5% difference in specimen capacity between grooves formed in grout and cast-in-place grooves, the latter were used for simplicity as they did not require drilling holes into the flange. The CFRP straps were installed prior to loading but were not prestressed until later on. The CFRP tape was wrapped over a metal pad on the soffit of the beam and into the groove through the flange. The outermost layer of the strap was then welded to the next outermost layer, creating a closed outer loop. A schematic diagram of this configuration is shown in **Fig. 1**.

The steel pad used to prestress the strap had four tapped holes drilled in the corners. Threaded rods fastened into these holes connected the pad to a prestressing rig composed of a hydraulic jack, a load cell, and a reaction frame. When the hydraulic jack is loaded, the load is transferred to the strap by the threaded rods/pad system while being read by the load cell. This load created a gap between the pad and the beam soffit. Metal inserts were then placed into this gap to maintain the strap under tension and the prestressing rig was removed. Strain gauges attached to the straps ensured that they carried the required force when the prestressing rig was detached. All straps were prestressed to a force of 22.5 kN (5.06 kips) which represented 25% of the ultimate strap capacity. This value was based on previous work by Kesse and Lees[7], and Hoult and Lees[8] who found that this level of prestress provided a balance between taking advantage of the beneficial effects of the prestress, and ensuring that there was a sufficient residual strap capacity to carry stresses due to crack openings.

Loading patterns

Three loading schemes were adopted for testing. Loading Pattern 0 (LP0) consisted of loading the beams up to failure. Loading Pattern 1 (LP1) and Loading Pattern 2 (LP2) involved initially pre-cracking the test specimens, using a load level of about 70% of the unstrengthened shear capacity, to model the state of damage that may exist in RC structures requiring strengthening. The beams were then unloaded to 40% of the unstrengthened capacity to mimic the residual dead load and the CFRP straps were prestressed. The final phase involved loading the strengthened beams up to failure. The main difference between LP1 and LP2 was that in LP1 the locations of the loads remained fixed through the loading sequence, so that the shear cracks formed on initial loading were likely to be mobilized once strengthened. Specimens subjected to LP2 were initially loaded to 70% of the unstrengthened capacity and unloaded to 40% of the unstrengthened capacity at position (B), as shown in **Fig. 2**. The CFRP straps were then prestressed and, although the total load was maintained, the load was shifted from position (B) to position (A). The specimen was then loaded to failure. Hence LP2 aims to stimulate different shear crack patterns before and after strengthening.

Test setup and instrumentation

U/295/LP0/4.5, S/215/LP1/4.6 and S/215/LP2/4.6 represented a single specimen tested in four-point bending. To speed up the testing process, U/295/LP2/4.5, S/295/LP1/4.5 and S/295/LP2/4.5 were tested in three-point bending to allow two tests to be carried out on a single beam. This was achieved by testing one beam end zone while keeping the other end overhung and unstressed and vice versa (see **Fig. 2**). In these beams, the 925 mm (36.41 in.) long shear span was reinforced with additional transverse steel reinforcement (Ø6 mm [Ø0.24 in.] shear links spaced at 100 mm [3.94 in.] center-to-center). For the strengthened beams S/295/LP1/4.5 and S/295/LP2/4.5, four additional prestressed CFRP straps spaced at 200mm (7.87 in.) center-to-center ensured that failure always occurred in the 1125 mm (44.29 in.) long shear span.

The deflections were measured with linear resistance displacement transducers (LRDTs), positioned either at mid-span for the beams tested in four-point bending or at position (A), i.e. at $a = 3.8d$, for the specimens tested in three-point bending. The strains were measured using strain gauges bonded to the internal transverse steel reinforcement, and to the outer CFRP strap layer, and were designated TR# and CF# respectively (see **Fig. 2**), where # indicates the strain gauge number. The LRDTs and strain gauge readings were acquired using an automatic data logging system.

EXPERIMENTAL RESULTS AND DISCUSSION

Shear force capacity

All the beams were tested to failure. The average cube compressive strength on testing day was 24.4 MPa (3.54 ksi) for all beams except S/215/LP1/4.6 which had a cube compressive strength of 32 MPa (4.65 ksi). **Table 1** gives the unstrengthened shear capacities as well as the shear forces at failure and the gains in shear capacity above the corresponding unstrengthened control beams. The unstrengthened control beam tested by Hoult and Lees[8], hereafter referred to as U/215/LP0/4.6(HL)[8], is nominally identical to S/215/LP1/4.6 and S/215/LP2/4.6 and will be used as a basis for comparison; it failed in shear at a shear force of approximately 88 kN (19.78 kips). The unstrengthened specimen U/295/LP0/4.5, which failed in shear at a shear force of 107 kN (24.05 kips), was used as a baseline standard for the 350 mm (13.78 in.) deep specimens. U/295/LP2/4.5, which failed in shear at a shear force of 116 kN (26.08 kips), was used to examine the effect of LP2 on the shear carrying capacity of an unstrengthened beam.

The 350 mm (13.78 in.) deep strengthened specimens S/295/LP1/4.5 and S/295/LP2/4.5 failed at a shear force of 136.4 kN (30.66 kips) and 136.5 kN (30.69 kN) respectively, attaining increases in shear force capacity of 27.5% and 27.6% respectively. The corresponding 270 mm (10.63 in.) deep strengthened specimens (S/215/LP1/4.6 and S/215/LP2/4.6) failed at a shear force of 128.5 kN (28.89 kips) and 107.0 kN (24.05 kips) respectively, achieving increases of 46% and 21.6% respectively above U/215/L0/4.6(HL)[8].

Apart from the case of the 270 mm (10.63 in.) deep strengthened specimens, the two load histories investigated, LP1 and LP2, did not generally seem to have a significant effect on the shear capacity of the tested beams. There was about 8% capacity difference in the unstrengthened beams and the 350 mm (13.78 in.) deep strengthened beams did not show any significant difference in capacity. During testing, it was clear that pre-existing cracks were interacting with subsequent crack formation, yet interestingly this interaction did not seem to impact greatly on the peak load at failure. The 270 mm (10.63 in.) deep strengthened beam S/215/LP1/4.6 achieved an increase of 40.5 kN (9.11 kips) above the control beam U/215/LP0/4.6(HL)[8], approximately double the 19 kN (4.27 kips) increase in shear capacity recorded in S/215/LP2/4.6. However, the former had a higher cube compressive strength (32 MPa [4.65 ksi]) than the latter (25 MPa [3.54 ksi]). Hence, it is difficult to judge whether the difference in the shear force capacity is due to the variation in loading and/or the concrete strength. A numerical (finite element) study reported later in this paper will investigate this aspect in more detail.

The effect of beam depth on the shear force capacity can be examined by considering the strap-strengthened beams subjected to LP2. The shear force capacity increased from 107 kN (24.05 kips) to 136.5 kN (30.69 kips) when the effective beam depth was increased from 215 mm (8.46 in.) to 295 mm (11.61 in.). Similarly, the contribution of the CFRP strap system to the shear force capacity increased from 19 kN (4.27 kips) to 29.5 kN (6.64 kips) with the increase in effective beam depth. The nominal shear stress at failure ($V_{exp}/b_w d$) decreased slightly from 4.7 MPa (0.68 ksi) to 4.4 MPa (0.64 ksi) with the increase in effective beam depth. This result suggests that the increase in effective beam depth was not accompanied by significant size effects.

Shear force-deflection relationships

Fig. 3 presents the shear force-deflection curves for the experimental specimens and also U/215/LP0/4.6(HL)[8]. All specimens experienced a drop in load at peak shear force which is a characteristic of brittle (shear) failure. Both U/295/LP0/4.5 and U/215/LP0/4.6(HL)[8] had initial

linear shear-deflection relationships. Under increased loading, the beams stiffness started to deteriorate and the shear-deflection curves turned nonlinear due to cracking. On further loading, cracking became more severe and the stiffness continued to deteriorate until eventually failure occurred. Beam U/295/LP2/4.5 showed a stiffer response compared to U/295/LP0/4.5 because it had a shorter beam length (see **Fig. 2**). During the first loading phase in position B, the shear force-deflection relationship was initially linear up to a shear force of approximately 55 kN (12.36 kips). At this load level, the shear force-deflection relationship turned nonlinear due to cracking. After unloading, the load was gradually shifted to position A which relieved the load applied at the initial position. Throughout the second loading phase, the beam stiffness continued to deteriorate due to cracking until finally failure occurred.

During the initial loading stage, the strengthened beams behaved similarly to the corresponding unstrengthened specimens. The beams subjected to LP2 had a higher initial stiffness compared to the beams subjected to LP1. This is due to the fact that the former beams were initially loaded at a shorter shear span. However, when all the beams were loaded at the same distance from the support in the final loading stage, the beams with the same lengths showed comparable stiffness.

The unstrengthened beams were more brittle compared to the corresponding strengthened beams. The average ratio of the total deflection at peak load between the strengthened beams and the corresponding unstrengthened beams, however, is of the same order of magnitude, about 1.80.

Failure mode

The two unstrengthened beams failed in shear as shown in **Fig. 4**. U/295/LP0/4.5 failed due to an inclined crack that ran from the support to the load point at an angle of approximately 24° in the web and a much shallower path in the flange. Specimen U/295/LP2/4.5 failed due to an inclined crack that penetrated the flange and propagated towards the load pad. This was accompanied by the excessive opening of one of the inclined cracks in the web. Of importance is that the inclined shear

cracks that formed in the first stage of loading remained stable and did not contribute to the failure mechanism. This may explain why load case LP2 had little effect on the shear carrying capacity.

The crack pattern at failure for the strengthened beams is shown in **Fig. 5**. In S/295/LP1/4.5, the main shear crack had two branches in the beam web. The first branch started at the support at an angle of approximately 26° and then turned approximately horizontal. It then crossed the outer strap and joined the second branch which started at the base of the outer strap. The second branch of the main shear crack propagated from the base of the outer strap towards the web-flange interface at an angle of approximately 31°. The flange suffered significant damage at failure. The failure mode also included a horizontal crack running back from the load pad.

A set of vertical cracks can be seen in the flange of S/295/LP2/4.5 close to the supports. This set of cracks started at the top of the flange and then propagated downwards. This phenomenon can be explained by strain compatibility between the flange and the web. With increased loading, the web portion between the support and the major shear crack attempts to rotate. However, the flange restrains its movement. Consequently, horizontal tensile strains and stresses develop in the top part of the flange. Eventually, the stresses exceed the concrete tensile strength and vertical cracks form.

Specimen S/215/LP1/4.6 suffered a shear failure due to a set of parallel shear cracks emerging from the support as well as above. The web cracks turned into a shallower angle in the flange where they joined to form a single crack that ran to the load pad. This was accompanied by significant damage in both the flange and the end of the beam. This is rather curious and local effects such as the reinforcement concentration may have led to the splitting of the end region.

The failure mode of specimen S/215/LP2/4.6 is also shown in **Fig. 5**. The shear crack that caused failure is traced for clarity. This shear crack emanated from the base of the outer strap and ran at an angle of approximately 34° towards the flange. It crossed the middle strap just under the flange, propagating horizontally along the web-flange interface before penetrating the flange and proceeding to the load pad. The flange suffered less damage in this specimen than in S/215/LP1/4.6.

The width of shear cracks was not measured as it was expected that very limited size effect – which may be defined as the reduction in shear strength of deeper sections attributable to wider shear cracks – existed due to the limited increase in beam depth from 270 mm (10.63 in.) to 350 mm (13.78 in.). This expectation was confirmed by the experimental results. As discussed in a previous section, S/215/LP2/4.6 and S/295/LP2/4.6, which differed in beam depth only, had nominal shear stresses ($V_{exp}/b_w d$) at failure of 4.7 MPa (0.68 ksi) and 4.4 MPa (0.64 ksi) respectively.

Strain in the steel shear reinforcement

This section reports on the strain in the transverse steel reinforcement in the shear spans where failure occurred (see **Fig. 6**). For the purpose of interpreting results, the shear links are categorized as "outer links" (TR1), "middle links" (TR2 and TR3 in the 350 mm [13.78 in.] deep specimens, and TR2 in the 270 mm [10.63 in.] deep specimens) and "inner links" (TR4 in the 350 mm [13.78 in.] deep specimens and TR3 in the 270 mm [10.63 in.] deep specimens). Unfortunately, some strain gauges failed during testing and their results were discarded.

The outer and middle shear links in the unstrengthened beams started to function only after a shear force of between 30 kN (6.74 kips) and 45 kN (10.12 kips). Thereafter, the strain in the stirrups increased significantly with increasing load. Most of the shear links in this group attained their yield strain after a shear force of approximately 90 kN (20.23 kips). This was expected since these links were crossed by the major shear cracks. The outer shear links in the strengthened specimens did not develop any significant strains until they were crossed by the inclined cracks. During the pre-cracking stage, they started to develop strains at a rate comparable to, or less than, the outer shear link in U/295/LP0/4.5. However, after the CFRP straps were prestressed and started to share the load with the steel links, the outer shear links in the strengthened specimens developed strains at a relatively low rate compared to the outer shear link in U/295/LP0/4.5. The strains in the middle shear links of the strengthened beams were negligible until the formation of the inclined cracks. After the prestressing of the CFRP straps, the middle shear links in the strap-strengthened beams

had a stiffer response than the corresponding shear links in U/295/LP0/4.5. The middle shear links carried the highest strains at failure. Most of the links in this group yielded prior to failure. This is due to the fact that the main shear cracks always crossed this group of shear links. The inner links carried the least amount of strain in all test specimens. These links were located in a region that did not experience much inclined cracking and the strains in this group of transverse reinforcement developed at a relatively low rate even after the formation of shear cracks.

Some of the mechanisms by which the CFRP straps increase the shear capacity can be understood from **Fig. 6**. The incorporation of the CFRP straps reduces the strain in the shear links, which is a measure of shear crack widths, due to prestressing and load sharing. Consequently, the external load required to progress existing cracks increases and this in turn enhances the shear capacity.

Strain in the CFRP straps

The shear force-strain curves for the CFRP straps in the shear spans where failure occurred are also shown in **Fig. 6**. The straps are categorized as "outer straps" (CF1), "middle straps" (CF2) and "inner straps" (CF3). The outer strap of S/215/LP1/4.6 experienced the highest ultimate strain. This was quite compatible with the failure mode of that specimen since two major shear cracks crossed that strap, forcing the strap to develop high strain. The remaining three outer straps were not crossed by major shear cracks and hence did not develop strains comparable to the strain developed in the outer strap of S/215/L1/4.6. The middle straps developed significantly higher strains compared to both the outer straps, with the exception of S/215/LP1/4.6/CF1, and the inner straps. **Fig. 6** shows that the middle straps in the specimens subjected to LP2 experienced higher strains at failure than the middle straps in the specimens subjected to LP1. Once again, this matches the failure modes of the specimens subjected to LP2. In these specimens, only the middle straps contributed to resisting the major shear cracks. The inner straps of the 270 mm (10.63 in.) deep specimens developed the least amount of strain at failure. This was to be expected since very few cracks crossed these straps. **Fig. 6** shows that the inner straps S/215/LP1/4.6/CF3 and S/215/LP2/4.6/CF3 carried about 300

micro-strain and 600 micro-strain at failure respectively. These strain values are comparable to the strain values experienced by the inner shear links. The corresponding straps in the 350 mm (13.78 in.) deep specimens resisted the main cracks penetrating the flange and therefore developed much higher strain. The inner straps S/295/LP1/4.5/CF3 and S/295/LP2/4.5/CF3 carried about 1500 micro-strain and 2300 micro-strain at failure respectively. It may be worth noting that the inner shear links in the 350 mm (13.78 in.) deep specimens were much closer to the loading point than the inner straps and they did not experience comparable strain to the inner straps as they were not crossed by major shear cracks. Based on the above discussion, it can be concluded that: (i) the inner straps, with the exception of S/295/LP1/4.5/CF3 and S/295/LP2/4.5/CF3, as well as the inner shear links carried the least amount of strain at failure, and (ii) the outer and middle straps, as well as the outer and middle shear links carried the highest strains at failure. Hence, the general trend of strap groups matched the trend exhibited by the corresponding shear link groups. The trends of both reinforcement systems were compatible with the observed failure modes.

FINITE ELEMENT MODELING

Load history and prestressed straps

Nonlinear finite element (FE) analyses were undertaken using the commercial FE package DIANA to support the experimental findings, incorporating the load history and modeling of the prestressed CFRP straps. Full details of the analytical studies can be found elsewhere[12].

Kesse et al.[13], Kesse[14] and Hoult[15] developed two dimensional FE models for RC beams transversely prestressed with the unbonded prestressed CFRP strap system. However, in all these numerical studies the straps were applied from the outset. In the following, analyses will be undertaken to represent the phased loading. The dependency of the strap strain results on the selected concrete shear model will also be considered by comparing the results from smeared crack analysis with (i) a fixed-angle crack model with constant shear retention factor, (ii) a fixed-angle crack model with nonlinear shear retention factor, or (iii) a total strain rotating-angle crack model.

Phased analysis, FE mesh and element details

Two-dimensional FE models were developed and examples are shown in **Fig 7**. The mesh size was taken as $2.5d_a$ where d_a is the aggregate size. This is broadly consistent with the recommendation of Bažant and Oh[16] ($3d_a$), and the element sizes used by Kesse[14] ($2d_a$ and $3d_a$) and Hoult[15] ($2.5d_a$). A half-model was developed for U/295/LP0/4.5, S/215/LP1/4.6 and S/215/LP2/4.6 since these beams were symmetric. The other beams were asymmetric and hence were fully modeled.

The concrete was modeled by the four-node plane stress elements Q8MEM[17]. The steel reinforcement was modeled as embedded reinforcement[17], by elements with no degrees of freedom of their own and strains computed from the displacement fields of the surrounding concrete elements. Bond failure between the concrete and the internal steel bars was not the governing failure mode of the tested specimens and so perfect bond was assumed between the concrete and the embedded steel reinforcement. There is still the potential for localized slip between the reinforcement and surrounding concrete in the tested beams, but this should not affect the overall predicted behaviour. For the strengthened beams, the strap system was included by adding two-node truss elements (L2TRU)[17]. As the CFRP straps were unbonded, the truss elements were connected only to the underside of the prestressing pads and the upper side of the beam. The steel support pads and prestressing pads were represented using the three-node plane stress elements T6MEM[17]. As there was no localized slip between the two pads and the beams, the T6MEM[17] elements were perfectly connected to the concrete elements. In order to allow for full rotation at the supports, the support pads were constrained against vertical translation at only one node. Appropriate boundary conditions were used as illustrated in **Fig. 7**.

DIANA Phased Analysis Module[17], which allows for the addition or removal of elements or boundary conditions between phases, was applied to model the staged addition of the FRP strengthening. However, as it was not possible to pre-stress the truss elements representing the CFRP straps, the initial pre-stress forces were applied as equal and opposite forces acting at the upper and lower nodes of the truss elements. Alternatively, it would have been possible to introduce

the prestressing forces using a fictitious thermal load. The set of three straps in specimens S/295/LP1/4.5 and S/295/LP2/4.5marked ¤ in **Fig. 7** was used to strengthen the tested shear span and was active in the last phase only. The set of straps marked ∗ in **Fig. 7** was used to strengthen the other shear span of the beam and was active during all phases.

Shear models

The smeared crack approach was implemented where the concrete is treated as a continuum even after cracking. In the fixed-angle crack model, a crack initiates perpendicular to the direction of the principal tensile stress according to the tension cut-off value used, its orientation remaining fixed. A successive crack is allowed to initiate at the same integration point as the initial crack, perpendicular to the new direction of the principal tensile stress, if the principal tensile stress exceeds the tension cut-off value and the angle between the new direction of the principal tensile stress and the existing crack exceeds a threshold angle (α_{TD})[17], taken as 60° in the current work. Based on DIANA[17] recommendations, this value was chosen to avoid the numerical instability caused by the formation of a large number of cracks at an integration point. Two shear retention models available in DIANA namely; a constant shear retention or a variable shear retention model, are used in this study. Specimens U/295/LP0/4.5, S/295/LP1/4.5 and S/295/LP2/4.5 were used to calibrate the constant shear retention factor: a value of 0.1 gave accurate predictions for the peak loads and the strain in the steel reinforcement and so was then adopted for all the other specimens. The variable shear retention model takes into account the dependency of the shear stiffness on the crack width. The associated parameters used in the variable shear retention model were selected based on DIANA[17] recommendations.

The rotating-angle crack model is a special case of the fixed-angle crack model with α_{TD} = 0°. The stress-strain relations are evaluated in the principal directions and the total strain model is based on the Modified Compression Field Theory[18]. A crack initiates in the rotating-angle crack model when the principal tensile stress exceeds the concrete tensile strength, and the crack direction changes

with a change in direction of the principal tensile stress. Thus the crack plane is a principal plane and shear stresses cannot exist on that plane so no concrete shear model is required.

Compression and tension models

Many of the selected material models were based on work by Kesse[14] and Hoult[15]. The models generally represented a balance between reflecting the behavior characteristics and complexity.

For the models using constant or variable shear retention factors, the Von-Mises yield criterion was used to govern concrete failure in compression and a compression stress-strain curve developed by Wang et al.[19] was implemented. For the rotating-angle models, the concrete in compression was modeled by Thorenfeldt's et al. stress-strain curve[17] which is predefined in DIANA total strain model[17]. However, Thorenfeldt et al.'s stress-strain curve becomes comparable to Wang et al.'s stress-strain curve for f_{cu} = 25 MPa (3.63 ksi) which is a reasonable approximation of the average cube compressive strength of the tested beams. Hence, the behavior of concrete in compression was similarly modeled in all FE models for a given beam. The concrete compressive and tensile strength properties used in the FE models for each beam were based on laboratory testing.

For initial cracking, a linear tension cut-off criterion was used and the post-cracking behaviour was modeled by a linear tension softening model that takes into account the gradual reduction in concrete tensile capacity. In DIANA[17], the linear tension softening model depends on the concrete tensile strength and the ultimate concrete tensile strain. The concrete tensile strength was determined experimentally whereas the ultimate concrete tensile strain was calculated based on DIANA[17] recommendations and previous work by Hoult[15] and Dirar[12]. Further details on the linear tension softening model are available elsewhere[17].

The support and pre-stressing pads, and the Ø8 mm (Ø0.31 in), Ø16 mm (Ø0.63 in), and Ø20 mm (Ø0.79 in) reinforcement bars, were modeled as elastic-perfectly plastic materials. But since the tensile test stress-strain curves of the Ø6 mm (Ø0.24 in) and Ø25 mm (Ø0.98 in) bars did not have a well-defined yield plateau, these bars were modeled as materials with plastic hardening. The Von-

Mises yield criterion was implemented in the plastic region. The CFRP straps were modeled as elastic brittle materials. The convergence criterion was based on force convergence.

FE results and comparison with experimental findings

The experimental and FE shear forces at failure are given in **Table 1**. The FE predictions were in broad agreement with the experimental results. The rotating-angle crack model (V_{rotat}) tended to slightly underestimate the shear forces at failure for LP0 and LP1 but slightly overestimate the failure forces for LP2. The fixed-angle crack model with variable shear retention factor (V_{var}) mostly overestimated the shear forces at failure, in particular 32% higher than experimental for S/215/LP2/4.6. This suggests that DIANA variable shear retention model overestimates the transfer of shear stresses across cracks. The fixed-angle crack model with constant shear retention factor (V_{const}) slightly overestimated some, and slightly underestimated others, of the shear forces at failure which suggests that the constant shear retention value of 0.1 considered in this study is reasonable.

Experimental and FE shear force-deflection curves for the 350 mm (13.78 in) deep beams are compared in **Fig. 8**. These curves show that the FE models predicted the initial uncracked stiffness accurately, suggesting that the elastic constants and boundary conditions were well modeled. However, in general, the FE predictions of the post-cracking stiffness deviated from the experimental. For U/295/LP0/4.5, both the constant and variable shear retention models overestimated the post-cracking stiffness whereas the rotating crack model slightly underestimated the post-cracking stiffness. Further, the peak deflections predicted by the constant and variable shear retention models were respectively 13% and 15.5% higher than the experimental peak deflection of 19.3 mm. For U/295/LP2/4.5, all the FE models overestimated the post-cracking stiffness by approximately 33%. This is suspected to be directly influenced by DIANA unloading model which assumes linear unloading from any point in the softening branch of the tension softening curve to the origin. Such a model does not take into account the permanent deformations of cracked concrete and hence may lead to overestimating the post-cracked stiffness in analyses

consisting of unloading-reloading cycles. All the FE models underestimated the post-cracking stiffness of S/295/LP1/4.5. Larger differences were noted with LP2 where, at approximately 80% of the peak shear force, the FE models for S/295/LP2/4.5 started to overestimate the stiffness. Full details of the predicted crack patterns and internal steel strains can be found elsewhere[12].

The predicted and experimental shear force-strain curves for the external CFRP straps for the 350 mm (13.78 in.) deep beams are presented in **Fig. 9**. The strain due to prestress of the CFRP straps is excluded. The FE models correctly predicted that the external CFRP straps resist the further opening of existing shear cracks and hence start to develop strain with increased loading. However, the shear forces at which the CFRP straps started to develop strain, and the variation of strain with shear force thereafter, were not well modeled. The perceived cause of these discrepancies is that the strain in the external CFRP straps depends on the strain in the concrete elements and none of the constitutive models effectively represented the actual behaviour of concrete in shear.

Investigation of influence of concrete strength

As mentioned previously, the concrete used in beam S/215/LP1/4.6 differed from that of S/215/LP2/4.6. FE models for S/215/LP1/4.6 were re-analyzed with the cube compressive strength taken as 25 MPa (3.63 ksi), i.e. similar to S/215/LP2/4.6. The rotating crack model predicted that the shear force at failure was 95.1 kN (21.38 kips) whereas the variable and constant shear retention models predicted that the shear forces were 108 kN (24.28 kips) and 100 kN (22.48 kips) respectively. The predicted results suggest that the reduction in the cube compressive strength is accompanied by a drop in the value of the shear force at failure. Hence, the difference in the shear carrying capacity between S/215/LP1/4.6 and S/215/LP2/4.6 was probably caused by the variation in the cube compressive strength rather than the loading patterns. This is in line with the other experimental results which suggested that the loading patterns did not generally seem to have a significant effect on the shear force carrying capacity.

Discussion and summary of FE results

The FE analyses helped support the interpretation of the experimental results. Although the results depended on the concrete modeling, general trends such as the overall load-deflection behavior and the implications of the phased loading could be identified. The FE modeling also facilitated initial investigations into the possible effects of a variation in the experimental parameters e.g. concrete strength. However, it was evident that the constant shear retention, the variable shear retention, and the rotating crack models, all had limitations in terms of predicting the strap strain at higher load levels. Furthermore, the models appeared to be less accurate in capturing the behavior when the beam was reloaded in a different location, as was the case with LP2. An investigation of the underlying reasons for these discrepancies is the subject of further work.

CONCLUSIONS

This study presents results of an experimental and FE investigation on the structural behavior of precracked RC T-beams strengthened in shear with unbonded prestressed CFRP straps. It also provides insights into the influence of load history and beam depth on the structural behavior of the strengthened beams. The strengthened beams exhibited capacity enhancements of 21.6% to 46% compared to the equivalent unstrengthened beams, demonstrating the potential effectiveness of the prestressed CFRP strap system. Apart from the case of the 270 mm (10.63 in.) deep strengthened specimens, the differences between the two load histories investigated, LP1 and LP2, did not generally seem to have a significant effect on the shear force capacity of the tested beams. During testing it was clear that pre-existing cracks were interacting with subsequent crack formations yet this interaction did not seem to impact greatly on the peak load at failure. The difference in shear force enhancement between S/215/LP1/4.6 and S/215/LP2/4.6 is an important result because it highlights the possible effect of concrete strength on the shear force capacity of strap-strengthened beams. The shear force enhancement increased with the increase in effective beam depth. However, the nominal shear stress at failure was not affected significantly by the increase in effective beam

depth, suggesting these beams did not display significant size effects. The prestressed CFRP straps reduced the brittleness of shear failure and relieved the strain in the shear links. FE analyses provided insight into the experimental behaviour but the predictions of the external CFRP strap strains had some limitations. This was particularly evident when modeling the beams where the load position was changed during testing.

NOTATION:

a = shear span

b_f = flange width

b_w = web width

d = effective beam depth

d_a = aggregate size

f_{cu} = cube compressive strength

p = longitudinal reinforcement ratio

t_f = flange thickness

V_{const} = shear force at failure predicted by the constant shear retention model

$V_{\exp}$ = experimental shear force at failure

V_{rotat} = shear force at failure predicted by the rotating crack model

V_{var} = shear force at failure predicted by the variable shear retention model

α_{TD} = threshold angle; taken as 60°

REFERENCES

1. Pellegrino, C., and Modena, C., "Fiber-Reinforced Polymer Shear Strengthening of Reinforced Concrete Beams: Experimental Study and Analytical Modeling," *ACI Structural Journal*, V. 103, No. 5, 2006, pp. 720-728.

2. Sundarraja, M. C., and Rajamohan, S., "Strengthening of RC Beams in Shear Using GFRP Inclined Strips – An Experimental Study," *Construction and Building Materials*, Elsevier, The Netherlands, V. 23, No. 2, 2009, pp. 856-864.

3. Czaderski, C., and Motavalli, M., "Fatigue Behaviour of CFRP L-Shaped Plates for Shear Strengthening of RC T-beams," *Composites Part B: Engineering*, Elsevier, The Netherlands, V. 35, No. 4, 2004, pp. 279-290.

4. De Lorenzis, L., and Nanni, A., "Shear Strengthening of Reinforced Concrete Beams with Near-Surface Mounted Fiber-Reinforced Polymer Rods," *ACI Structural Journal*, V. 98, No. 1, 2001, pp. 60-68.

5. Motavalli, M., Czaderski, C., and Pfyl-Lang, K., "Prestressed CFRP for Strengthening of Reinforced Concrete Structures: Recent Developments at Empa, Switzerland," *ASCE Journal of Composites for Construction*, V. 15, No. 2, 2011, pp. 194-205.

6. Lees, J. M., and Winistörfer, A. U., "Nonlaminated FRP Strap Elements for Reinforced Concrete, Timber, and Masonry Applications," *ASCE Journal of Composites for Construction*, V. 15, No. 2, 2011, pp. 146-155.

7. Kesse, G., and Lees, J. M., "Experimental Behavior of Reinforced Concrete Beams Strengthened with Prestressed CFRP Shear Straps," *ASCE Journal of Composites for Construction*, V. 11, No. 4, 2007, pp. 375-383.

8. Hoult, N. A., and Lees, J. M., "Efficient CFRP Strap Configurations for the Shear Strengthening of Reinforced Concrete T-Beams," *ASCE Journal of Composites for Construction*, V. 13, No. 1, 2009, pp. 45-52.

9. Hoult, N. A., and Lees, J. M., "Time-Dependent Behavior of RC Beams Retrofitted with CFRP Straps," *ASCE Journal of Composites for Construction*, V. 15, No. 1, 2011, pp. 75-84.

10. Hoult, N. A., and Lees, J. M., "Modeling of an Unbonded CFRP Strap Shear Retrofitting System for Reinforced Concrete Beams," *ASCE Journal of Composites for Construction*, V. 13, No. 4, 2009, pp. 292-301.

11. Dirar, S., Lees, J., and Morley, C., "Precracked Reinforced Concrete T-Beams Repaired in Shear with Bonded Carbon Fiber-Reinforced Polymer Sheets," *ACI Structural Journal*, V. 109, No. 2, 2012, pp. 215-224.

12. Dirar, S. M. O. H., "Shear Strengthening of Pre-cracked Reinforced Concrete T-Beams Using Carbon Fibre Systems," PhD Thesis, University of Cambridge, 2009, 196pp.

13. Kesse, G., Chan, C., and Lees, J. M., "Nonlinear Finite Element Analysis of RC Beams Prestressed with CFRP Straps," *Proceedings of the 5th International Symposium on Fibre-reinforced Plastics for Reinforced Concrete Structures*, Vol. 1, 2001, pp. 281-290.

14. Kesse, G., "Concrete Beams with External Prestressed Carbon FRP Shear Reinforcement," PhD Thesis, University of Cambridge, 2003, 222pp.

15. Hoult, N. A., "Retrofitting of Reinforced Concrete Beams with CFRP Straps to Enhance Shear Capacity," PhD Thesis, University of Cambridge, 2005, 241pp.

16. Bažant, Z. P., and Oh, B. H., "Crack Band Theory for Fracture of Concrete," *Matériaux et Constructions*, Springer, The Netherlands, Vol. 16, No. 93, 1983, pp. 155-177.

17. TNO DIANA BV, "DIANA (Release 9.2) User's Manual", Delft, The Netherlands, 2007.

18. Vecchio, F. J., and Collins, M. P., "The Modified Compression-Field Theory for Reinforced Concrete Elements Subjected to Shear," *ACI Structural Journal*, Vol. 83, No. 2, 1986, pp. 219-231.

19. Wang, P. T., Shah, S. P., and Naaman, A. E., "Stress-Strain Curves of Normal and Lightweight Concrete in Compression," *ACI Structural Journal*, Vol. 75, No. 11, 1978, pp. 603-611.

TABLES AND FIGURES

List of Tables:

List of Figures:

Table 1–Experimental and FE predicted results

Specimen	Unstren-gthened shear capacity, kN (kips)	Shear force at failure (V_{exp}), kN (kips)	Gain in shear strength, kN (kips)	Gain in shear strength, %	V_{rotat}, kN (kips)	V_{rotat} / V_{exp}	V_{var}, kN (kips)	V_{var}/ V_{exp}	V_{const}, kN (kips)	V_{const} / V_{exp}
U/295/LP 0/4.5	107.0 (24.05)	107.0 (24.05)	0 (0)	0	93.3 (20.97)	0.87	123.0 (27.65)	1.15	119.0 (26.75)	1.11
U/295/LP 2/4.5	107.0* (24.05)	116.0 (26.08)	9.0 (2.03)	8.4	127.0 (28.55)	1.09	100.4 (22.57)	0.87	97.3 (21.87)	0.84
S/295/LP 1/4.5	107.0 (24.05)	136.4 (30.66)	29.4 (6.61)	27.5	118.0 (26.53)	0.87	142.0 (31.92)	1.04	135.0 (30.35)	0.99
S/295/LP 2/4.5	107.0 (24.05)	136.5 (30.69)	29.5 (6.64)	27.6	143.0 (32.15)	1.05	148.0 (33.27)	1.08	114.0 (25.63)	0.84
U/215/LP 0/4.6(HL)	88.0** (19.78)	88.0** (19.78)	0 (0)	0	–	–	–	–	–	–
S/215/LP 1/4.6	88.0** (19.78)	128.5 (28.89)	40.5 (9.11)	46.0	102.0 (22.93)	0.79	125.0 (28.10)	0.97	113.0 (25.40)	0.88
S/215/LP 2/4.6	88.0** (19.78)	107.0 (24.05)	19.0 (4.27)	21.6	122.0 (27.43)	1.14	141.0 (31.70)	1.32	125.0 (28.10)	1.17
Average predicted to experimental shear strength ratio						**0.97**		**1.07**		**0.97**
Standard deviation						**0.14**		**0.15**		**0.14**

* For purpose of comparison with U/295/LP0/4.5.

** Based on the control beam, tested by Hoult and Lees[8], which is nominally identical to S/215/LP1/4.6 and S/215/LP2/4.6.

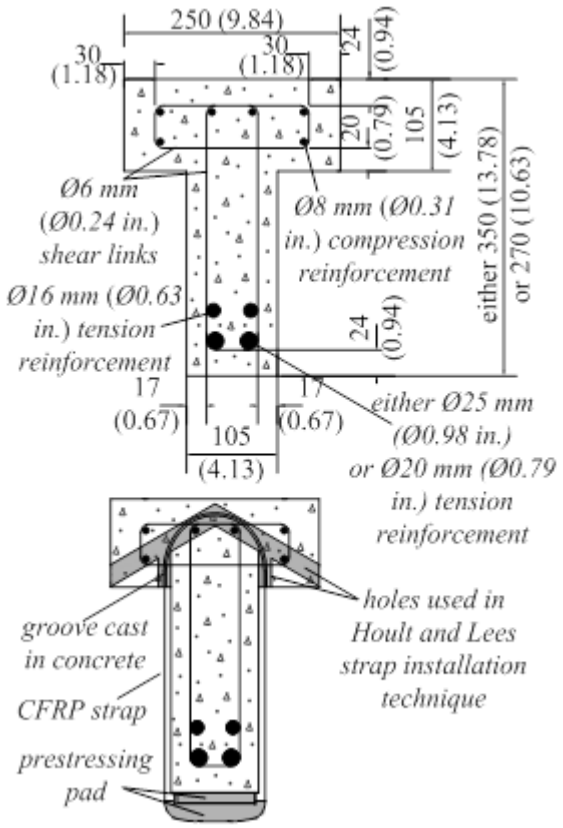

Fig. 1– Cross-sections – dimensions in mm (in.)

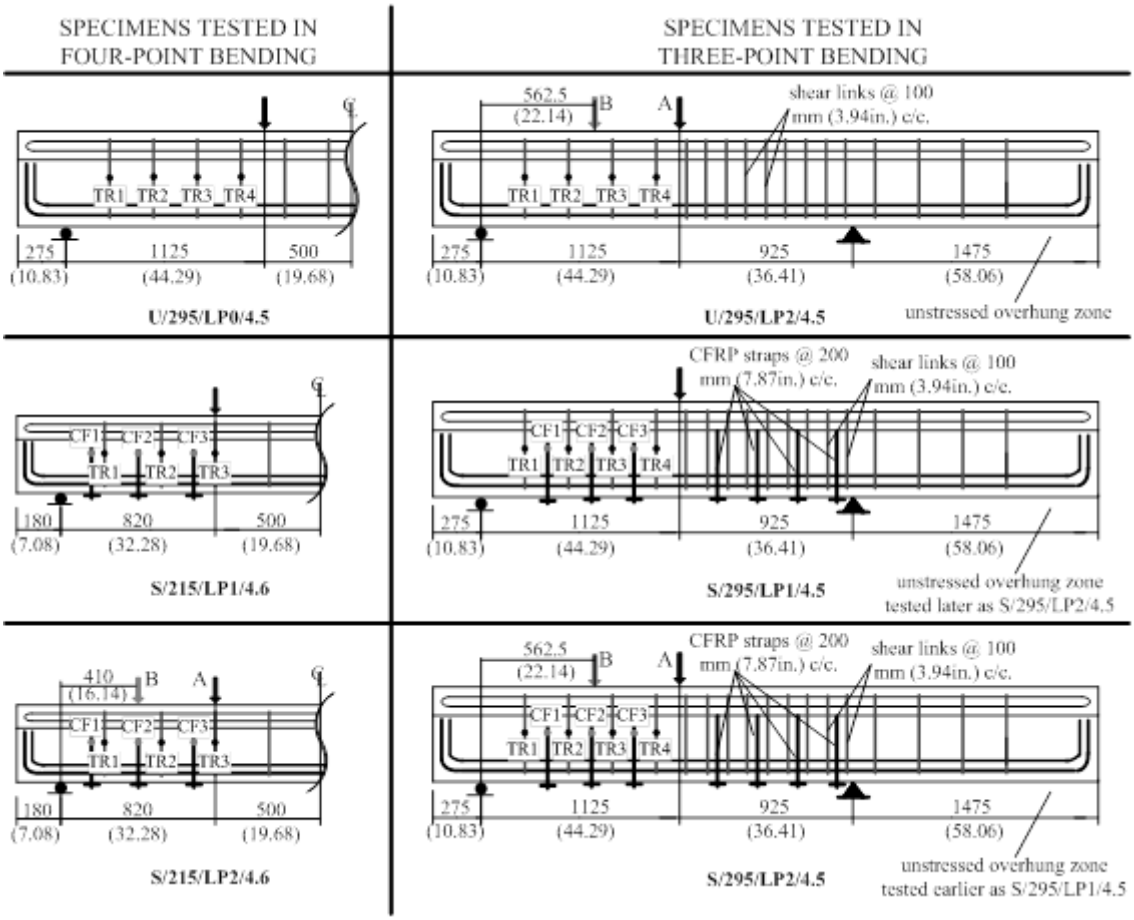

Fig. 2– Details of test specimens and loading patterns – dimensions in mm (in.).

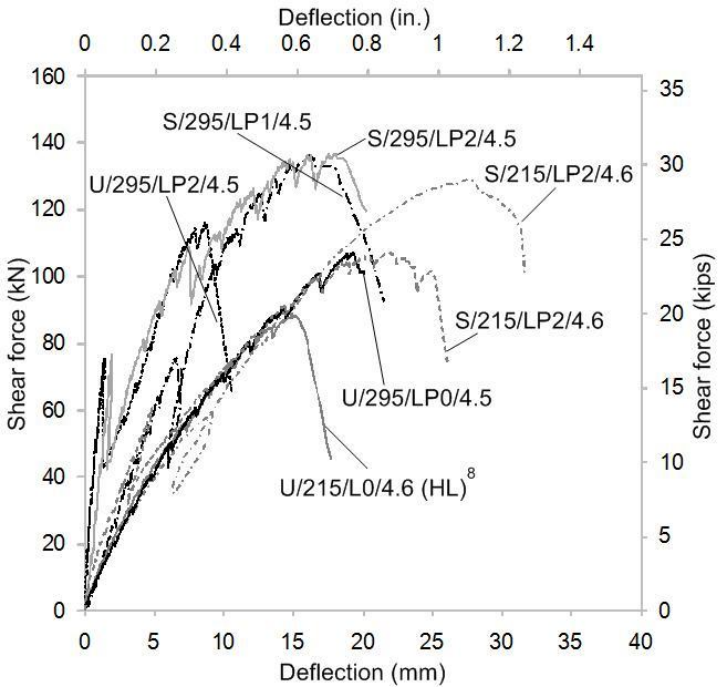

Fig. 3– Shear force-deflection curves.

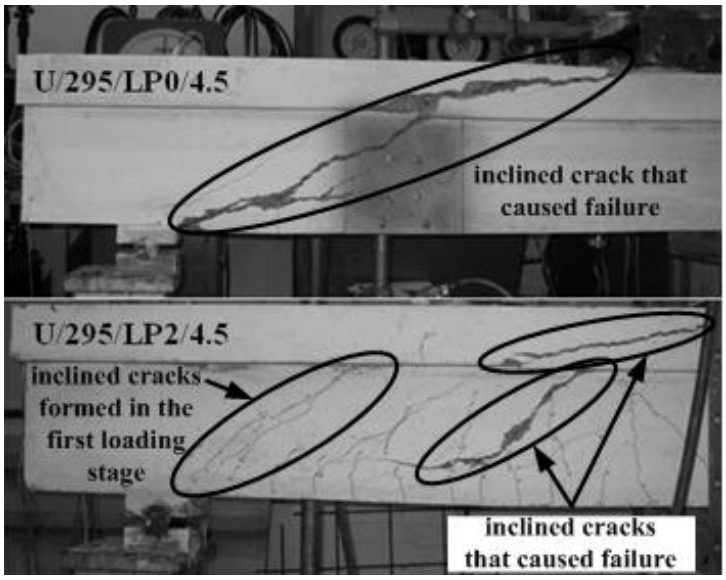

Fig. 4– Unstrengthened specimens at failure.

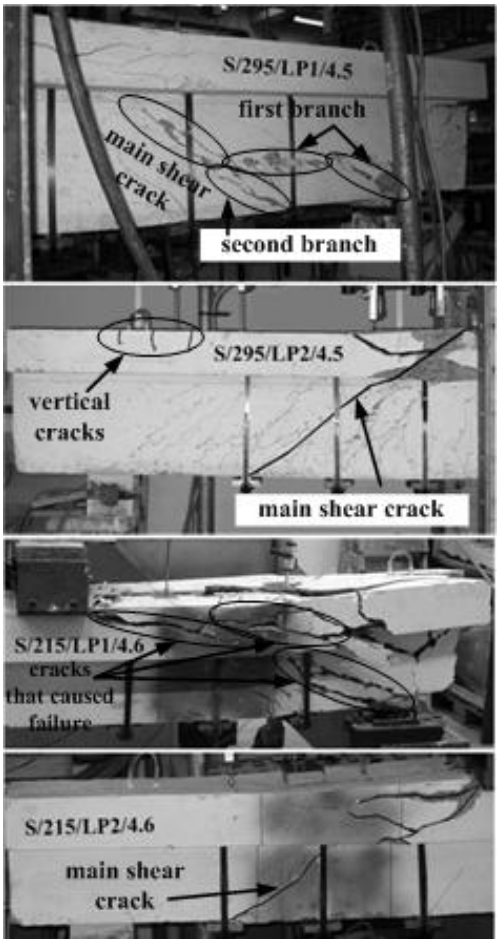

Fig. 5– Strengthened beams at failure.

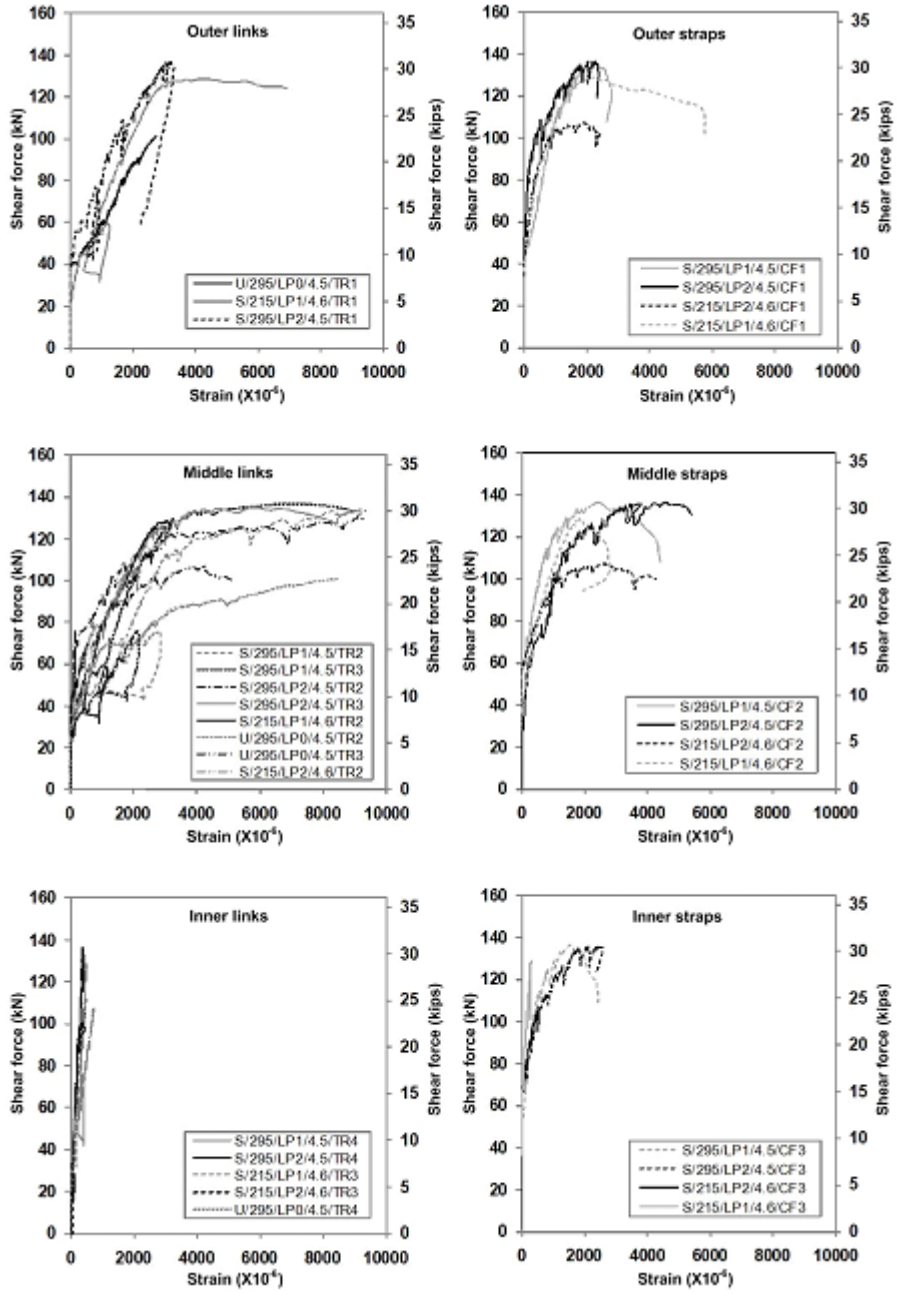

Fig. 6– Shear force versus strain in the internal shear and external CFRP reinforcement.

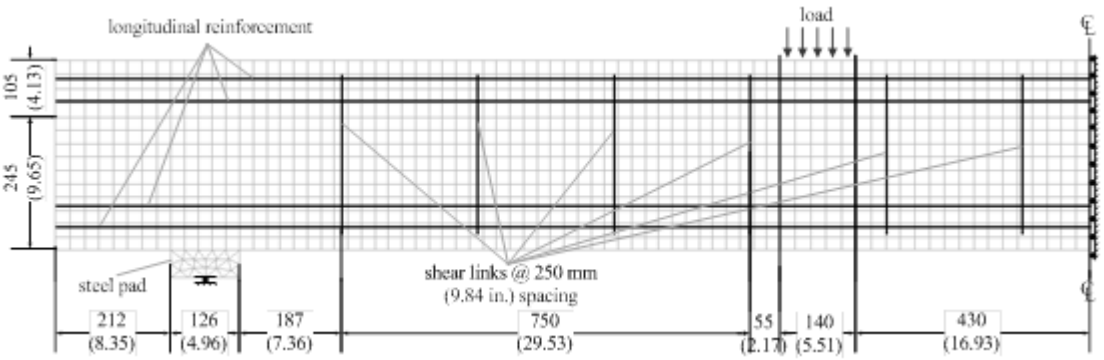

(a) U/295/LP0/4.5

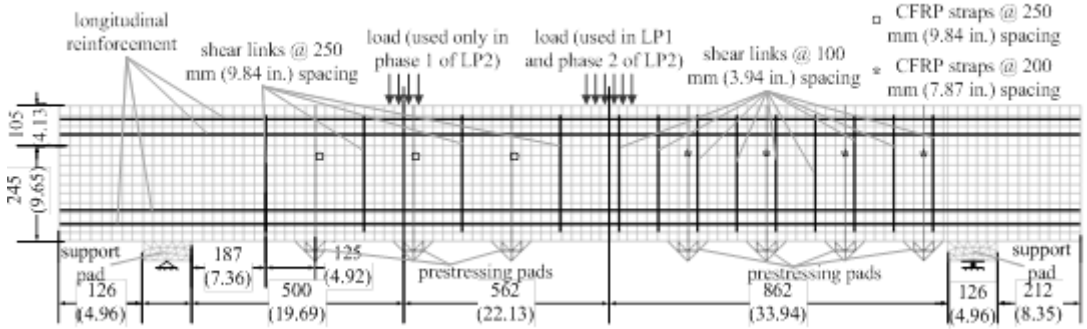

(b) S/295/LP1/4.5 and S/295/LP2/4.5

Fig. 7– Typical FE meshes with support and loading conditions – all dimensions in mm (in.)

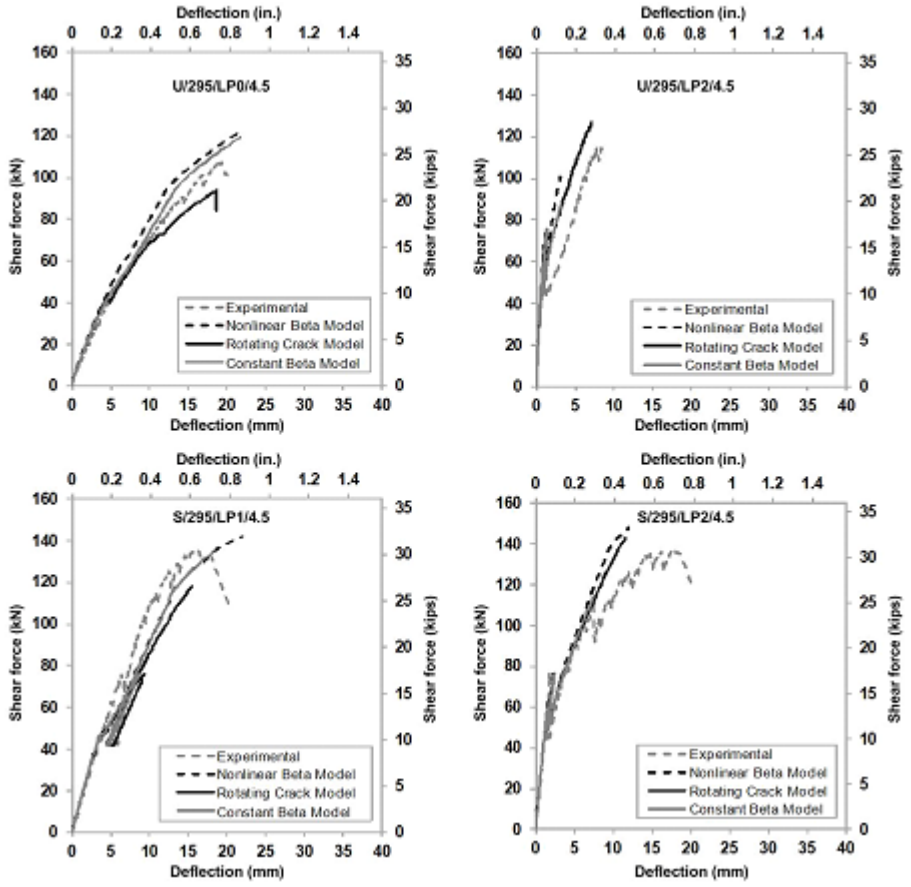

Fig. 8– Predicted and experimental shear force-deflection curves

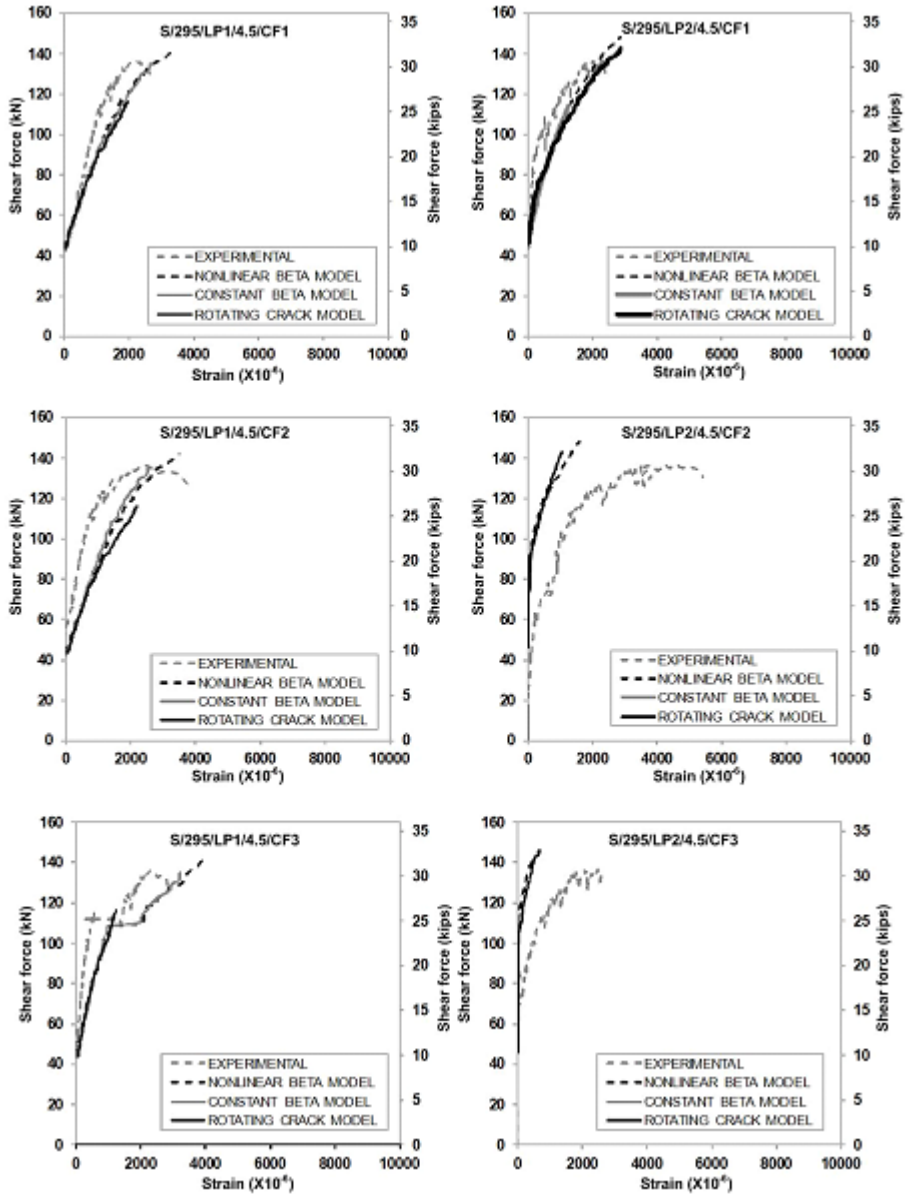

Fig. 9– Predicted and experimental shear force-strain curves for the straps